Fortschritte der Physik

Progress of Physics

WILEY-VCH

REPRINT

Cooperativity in light scattering by cold atoms

Tom Bienaimé[1]**, Romain Bachelard**[2]**, Nicola Piovella**[3]**,** and **Robin Kaiser**[1,*]

[1] Université de Nice Sophia-Antipolis, CNRS, Institut Non Linéaire de Nice, UMR 7335, 06560 Valbonne, France
[2] Instituto de Física de São Carlos, Universidade de São Paulo, 13560-970 São Carlos, SP, Brazil
[3] Dipartimento di Fisica, Università Degli Studi di Milano, Via Celoria 16, 20133 Milano, Italy

A cloud of cold N two-level atoms driven by a resonant laser beam shows cooperative effects both in the scattered radiation field and in the radiation pressure force acting on the cloud center-of-mass. The induced dipoles synchronize and the scattered light presents superradiant and/or subradiant features. We present a quantum description of the process in terms of a master equation for the atomic density matrix in the scalar, Born-Markov approximations, reduced to the single-excitation limit. From a perturbative approach for weak incident field, we derive from the master equation the effective Hamiltonian, valid in the linear regime. We discuss the validity of the driven timed Dicke ansatz and of a partial wave expansion for different optical thicknesses and we give analytical expressions for the scattered intensity and the radiation pressure force on the center of mass. We also derive an expression for collective suppression of the atomic excitation and the scattered light by these correlated dipoles.

1 Introduction

Cooperative scattering by large collections of resonant atoms has been studied extensively for many years adopting either a classical or a quantum description. Often a quantum formalism is more convenient to describe the atom-light interaction. For instance, superradiant emission can be obtained when many independent atoms interact resonantly with photons, as studied in the seminal work by Dicke [1]. However, many features can well be described with classical models for the atoms with a polarizability and for the light field. Many features of Dicke superradiance can thus be explained using classical theory. As atoms appear to be excellent systems to study any possible deviation from classical many body features, it is of general interest to understand and to monitor cooperative effects, even at a classical level, in a cloud of atoms. New intriguing effects can arise, when fluctuations due to the coupling with the vacuum modes can no longer be described by a classical field approach and the atoms can also become entangled during the cooperative scattering. Such cooperative scattering with atomic ensembles can appear in a number of experimental situations in free space [2] or in cavities [3].

Collective spontaneous emission at single excitation level [1] has also been studied in resonant nuclear scattering of synchrotron radiation [4,5] and has recently received growing interest with the study of single photon superradiance from N two-level atoms prepared by the absorption of a single photon [6–9]. It has been shown that the photon is spontaneously emitted in the same direction as the incident field with a cooperative decay rate proportional to N and inversely proportional to the size of the atomic cloud [8]. In a series of theoretical [10] and experimental [11, 12] studies, the authors have recently addressed the question of the quasi-resonant interaction of light with clouds of cold atoms, bridging the gap from single

* Corresponding author E-mail: robin.kaiser@inln.cnrs.fr, Phone: +33 (0)4 92 96 73 91, Fax: +33 (0)4 92 96 73 33

atom behavior, with granularity effects due to the discrete nature of the atomic distribution, to a 'mean-field' regime, where a continuous density distribution is the relevant description and leads to cooperative effects. In these works, the authors describe the collective atomic response under continuous excitation of a low intensity light field using an effective Hamiltonian model valid in the linear regime. From it, the average radiation pressure force and the scattered intensity have been derived, observing the modification from the single-atom values due to cooperativity [13].

In this paper, we present an extended model based on a master equation in the single-excitation approximation. Such model provides a more complete description of the linear regime, useful to investigate the distinctions between classical and quantum features, even though a complete description of quantum correlations in our system requires to take into account a larger number of excitations [14, 15]. In particular, we show that by a first-order perturbation expansion of the master equation we recover the previously adopted linear model for classical optics. We also derive an analytical expression showing the cooperative suppression of atomic excitation and the related fluorescence. This effect bears some common features with the dipole blockade studied in Rydberg systems [16–18]. In our case the long range $1/r$ dipole-dipole coupling is at the origin of this important suppression even for dilute clouds of cold atoms. We note that this suppression occurs in the linear optics regime and is thus not related to a photon blockade.

2   The master equation approach

2.1   The exact master equation for driven atoms

The dynamics of a system of atoms driven by an external laser beam and undergoing cooperative re-emission into vacuum modes (see Fig. 1) can be described by a master equation approach [19, 20]. Let us consider a system of N two-level atoms with transition frequency ω_a, positions $\mathbf{r}_j$ and excited decay time Γ. Each atom is described by the spin half angular momentum algebra, with $S_-^i = |g_i\rangle\langle e_i|$, $S_+^i = |e_i\rangle\langle g_i|$, $S_z^i = |e_i\rangle\langle e_i| - |g_i\rangle\langle g_i|$ satisfying the commutation relations $[S_+^i, S_-^j] = \delta_{ij} S_z^i$ and $[S_\pm^i, S_z^j] = \mp 2\delta_{ij} S_\pm^i$. The interaction Hamiltonian is

$$H = \frac{\hbar\Omega_0}{2} \sum_{j=1}^N \left(S_-^j e^{i\Delta_0 t - i\mathbf{k}_0\cdot\mathbf{r}_j} + S_+^j e^{-i\Delta_0 t + i\mathbf{k}_0\cdot\mathbf{r}_j} \right)$$

$$+ \hbar \sum_{j=1}^N \sum_{\mathbf{k}} g_{\mathbf{k}} \left(S_-^j e^{i\omega_0 t} + S_+^j e^{-i\omega_0 t} \right) \left(a_{\mathbf{k}} e^{-i\omega_k t + i\mathbf{k}\cdot\mathbf{r}_j} + a_{\mathbf{k}}^\dagger e^{i\omega_k t - i\mathbf{k}\cdot\mathbf{r}_j} \right) \tag{1}$$

where $\Omega_0 = dE_0/\hbar$ is the Rabi frequency of the classical incident field with amplitude E_0 and wave vector $\mathbf{k}_0$, d is the dipole matrix element, $\Delta_0 = \omega_0 - \omega_a$ is the pump-atom detuning, $a_{\mathbf{k}}$ is the photon annihilation operator with wave number $\mathbf{k}$ and frequency $\omega_k = ck$, $g_{\mathbf{k}} = d[\omega_k/(2\hbar\epsilon_0 V_{ph})]^{1/2}$ and V_{ph} the photon volume. We have assumed the rotating wave approximation (RWA) in the first term accounting for the interaction with the external laser, but not in the second term: there, the coupling between atoms and vacuum field modes is described in the scalar light approximation, where near field and polarization effects are neglected, since we are considering dilute clouds, with $N(\lambda/R)^3 \ll 1$ (R the system size).

It has been shown in [19] that the spontaneous emission properties can be conveniently described by a reduced master equation for the atomic system in the Born-Markov approximation, given by

$$\frac{d\rho}{dt} = -i\frac{\Omega_0}{2} \sum_i \left[e^{i\Delta_0 t - i\mathbf{k}_0\cdot\mathbf{r}_i} S_-^i + e^{-i\Delta_0 t + i\mathbf{k}_0\cdot\mathbf{r}_i} S_+^i, \rho \right]$$

$$-i \sum_i \sum_{j\neq i} \Delta_{ij} [S_+^i S_-^j, \rho]$$

$$+ \frac{1}{2} \sum_i \sum_j \gamma_{ij} \left\{ 2S_-^j \rho S_+^i - S_+^i S_-^j \rho - \rho S_+^i S_-^j \right\}. \tag{2}$$
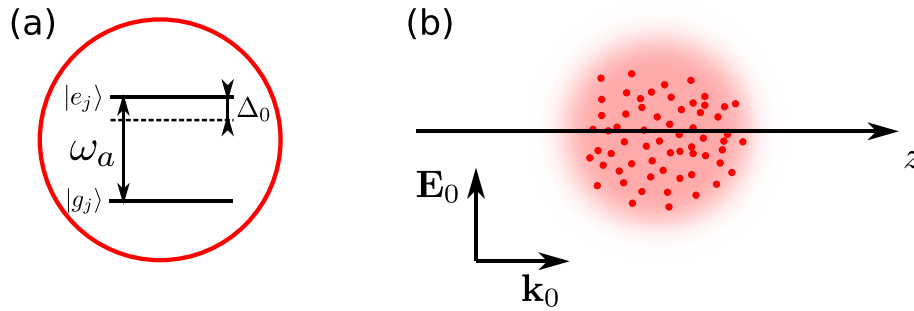
Fig. 1 (online colour at: www.fp-journal.org) Experimental configuration: a cloud of two-level atoms (a) is driven by an incident laser detuned by Δ_0 from the atomic resonance ω_a, with wave vector $\mathbf{k}_0$ (b).

where

$$\Delta_{ij} = -\frac{\Gamma}{2} \frac{\cos(k_0|\mathbf{r}_i - \mathbf{r}_j|)}{k_0|\mathbf{r}_i - \mathbf{r}_j|}, \tag{3}$$

$$\gamma_{ij} = \Gamma \frac{\sin(k_0|\mathbf{r}_i - \mathbf{r}_j|)}{k_0|\mathbf{r}_i - \mathbf{r}_j|}. \tag{4}$$

and $\Gamma = d^2 k_0^3/(2\pi\hbar\epsilon_0)$. The first term in the master equation (2) describes the interaction with the external laser. The second term describes the dipole-dipole interactions and arises from the virtual photon exchange between pairs of atoms. It becomes especially important at small interatomic distances, it is responsible for the collective Lamb shift [21, 22] and plays an important role in the subradiant emission [9, 23, 24]. Finally, the third term of Eq. (2) describes the cooperative emission. The Markov approximation ignores retardation effects and takes the long time limit, i.e. $t \gg 1/\omega_0$ and $t \gg \max\{|\mathbf{r}_i - \mathbf{r}_j|/c\}$. Hence, it requires that the system size is not too large, such that one photon travels through the atomic cloud faster than the characteristic cooperative emission time.

   The RWA approximation adopted in the present model requires more subtle arguments. As discussed in [19], when applied to the second term of the Hamiltonian of Eq. (1), the RWA consists in ignoring anti-resonant terms like $a_\mathbf{k}^\dagger S_+^j$ and $a_\mathbf{k} S_-^j$ which correspond to simultaneous creation or annihilation of a photon and atomic excitation (i.e. virtual transition). These terms are responsible of the shift of the ground state which contributes to the terms Δ_{ij} in Eq. (2). However, the master equation (2) has been obtained in [19] from the complete Hamiltonian (1) including the anti-resonant term, and making the RWA only on the master equation, neglecting the rapidly oscillating terms like $S_+^j \rho S_+^i e^{2i\omega_0 t}$. Hence, Eq. (2) obtained by making the RWA on the master equation rather than on the Hamiltonian does include the shift of the ground state. These remarks make clear that RWA on the Hamiltonian is not the same as RWA on the master equation and that one should make RWA on the final equations of motion. Since the counter-rotating terms as $S_+\rho S_+ e^{2i\omega_0 t}$ are not important because $\Gamma \ll \omega_0$, Eq. (2) provides an accurate description of the interaction, including both the contributions of the real and virtual transitions to the frequency shift.

2.2   Single-excitation approximation

The master equation (2) has been used to describe, in the absence of the driving laser, the superradiant and subradiant decays from excited atoms. For a system confined in a volume whose size is much smaller than the radiation wavelength, and neglecting the dipole-dipole interaction terms Δ_{ij}, Dicke [1] introduced the angular momentum states $|J, M\rangle = \text{Sym}\{|e \ldots e; g \ldots g\rangle\}$, with $M = -J, \ldots, J$. If the system is initially prepared in a symmetric (superradiant) state (with e.g. $J = N/2$), and in the absence of coupling to antisymmetric (subradiant) states, the radiative desexcitation occurs between symmetric states only. Note

however that the presence of dipole-dipole interactions may induce coupling with subradiant states [23]. In our case, the presence of the driving laser provides the atom excitation which subsequently scatters and/or decays cooperatively. If the driving field is sufficiently weak or largely detuned from the atomic resonance, we can assume that the atomic system is weakly excited, with at most one atom out of N excited. If the atoms are organized in a symmetric state, the decay rate is $N\Gamma$. Recently, it has been shown that an extended system of size $R \gg \lambda$ ($\lambda = 2\pi/k_0$ is the light wavelength) containing a single excited atom among N and prepared in the timed Dicke state [4, 6, 8, 25]

$$|TD\rangle = \frac{1}{\sqrt{N}} \sum_{j=1}^{N} \exp(i\mathbf{k}_0 \cdot \mathbf{r}_j) |g_1, \ldots, e_j, \ldots, g_N\rangle, \tag{5}$$

decays with a rate $\Gamma_N \propto N\Gamma/(k_0 R)^2$. Also, an external field Ω_0 drives the system mainly in a steady state of the form [10, 11]

$$|\Psi\rangle_N \approx |g_1, \ldots, g_N\rangle + \frac{\sqrt{N}\Omega_0 e^{-i\Delta_0 t}}{2\Delta_0 + i\Gamma(1 + b_0/12)} |TD\rangle, \tag{6}$$

where $b_0 = (3\lambda^2/2\pi) \int dz\, \rho(0,0,z) \propto N/(k_0 R)^2$ is the resonant optical thickness along the propagation direction z of the driving laser and $\rho(\mathbf{r})$ is the atomic density. However, a small fraction of the initial ground state is still coupled to the subradiant states, as discussed in [26].

The previous works studying cooperative scattering by weakly excited atoms were based on a effective Hamiltonian model and brought us to a description equivalent to that of N classical linear dipoles driven by the external field [10, 13]. Here, we go beyond the linear optics approximation using a master equation approach, still restricted to a single excitation. This restriction would be limited to the case of weak driving field, but may have a larger validity, for instance for Rydberg's atoms where some kind of blockade is provided [27].

By projecting Eq. (2) on the ground state $|G\rangle \equiv |g_1, \ldots, g_N\rangle$ and on the single-excitation states $|i\rangle \equiv |g_1, \ldots, e_i, \ldots, g_N\rangle$, neglecting the states containing more than one excitation and defining $\rho_{i,G} = \langle i|\rho|G\rangle \exp(i\Delta_0 t)$, $\rho_{G,G} = \langle G|\rho|G\rangle$ and $\rho_{i,j} = \langle i|\rho|j\rangle$, we obtain

$$\frac{d\rho_{G,G}}{dt} = -i\frac{\Omega_0}{2} \sum_k \left(e^{-i\mathbf{k}_0 \cdot \mathbf{r}_k} \rho_{k,G} - e^{i\mathbf{k}_0 \cdot \mathbf{r}_k} \rho_{G,k} \right) + \sum_{k,l} \gamma_{kl} \rho_{l,k}, \tag{7}$$

$$\frac{d\rho_{i,G}}{dt} = \left(i\Delta_0 - \frac{\Gamma}{2} \right) \rho_{i,G} - i\frac{\Omega_0}{2} \left(e^{i\mathbf{k}_0 \cdot \mathbf{r}_i} \rho_{G,G} - \sum_k e^{i\mathbf{k}_0 \cdot \mathbf{r}_k} \rho_{i,k} \right)$$
$$- \sum_{k \neq i} \left(\frac{\gamma_{ik}}{2} + i\Delta_{ik} \right) \rho_{k,G}, \tag{8}$$

$$\frac{d\rho_{i,j}}{dt} = -i\frac{\Omega_0}{2} \left(e^{i\mathbf{k}_0 \cdot \mathbf{r}_i} \rho_{G,j} - e^{-i\mathbf{k}_0 \cdot \mathbf{r}_j} \rho_{i,G} \right) - i \sum_{k \neq i} \Delta_{ik} \rho_{k,j} + i \sum_{k \neq j} \Delta_{kj} \rho_{i,k}$$
$$- \frac{1}{2} \sum_k \left(\gamma_{ik} \rho_{k,j} + \gamma_{kj} \rho_{i,k} \right). \tag{9}$$

We note that these equations still conserve the probability: $\rho_{G,G} + \sum_i \rho_{i,i} = 1$.

2.3   Perturbative solution

We now show that the effective Hamiltonian approach can be obtained by a perturbative expansion of ρ in terms of the Rabi frequency Ω_0 of the external field. Assuming $\rho = \rho^{(0)} + \rho^{(1)} + \ldots$, if initially the system

is in the ground state, the zero-order term yields $\rho_{G,G}^{(0)} = 1$ and $\rho_{i,G}^{(0)} = \rho_{i,j}^{(0)} = 0$, whereas at the first order, Eqs. (7)–(9) reduce to:

$$\frac{d\rho_{G,G}^{(1)}}{dt} = \sum_{k,l} \gamma_{kl} \rho_{l,k}^{(1)}, \tag{10}$$

$$\frac{d\rho_{i,G}^{(1)}}{dt} = \left(i\Delta_0 - \frac{\Gamma}{2}\right) \rho_{i,G}^{(1)} - i\frac{\Omega_0}{2} e^{i\mathbf{k}_0 \cdot \mathbf{r}_i} - \sum_{k \neq i} \left(\frac{\gamma_{ik}}{2} + i\Delta_{ik}\right) \rho_{k,g}^{(1)}, \tag{11}$$

$$\frac{d\rho_{i,j}^{(1)}}{dt} = -i\sum_{k \neq i} \Delta_{ik} \rho_{k,j}^{(1)} + i\sum_{k \neq j} \Delta_{kj} \rho_{i,k}^{(1)} - \frac{1}{2}\sum_{k} \left(\gamma_{ik}\rho_{k,j}^{(1)} + \rho_{i,k}^{(1)}\gamma_{kj}\right). \tag{12}$$

Since $\rho_{i,j}^{(1)}(0) = 0$, Eqs. (10) and (12) imply that at all times $\rho_{i,j}^{(1)}(t) = \rho_{G,G}^{(1)}(t) = 0$. The remaining Eq. (11) can be written defining $\beta_i = \rho_{i,G}^{(1)}$ and using Eqs. (3) and (4), as

$$\frac{d\beta_i}{dt} = \left(i\Delta_0 - \frac{\Gamma}{2}\right) \beta_i - i\frac{\Omega_0}{2} e^{i\mathbf{k}_0 \cdot \mathbf{r}_i} - \frac{\Gamma}{2}\sum_{k \neq i} \frac{\exp(ik_0|\mathbf{r}_i - \mathbf{r}_k|)}{ik_0|\mathbf{r}_i - \mathbf{r}_k|} \beta_k. \tag{13}$$

Furthermore, we observe that, since $\rho_{i,j} = \langle i|\rho|G\rangle\langle G|\rho|j\rangle + \sum_k \langle i|\rho|k\rangle\langle k|\rho|j\rangle$, the first non zero order for the dipole correlations corresponds to the second order for the field: $\rho_{i,j}^{(2)} = \rho_{i,G}^{(1)}\rho_{G,j}^{(1)} = \beta_i\beta_j^*$.

2.4 Effective Hamiltonian

Equation (13) can be expressed in the form of a Schrödinger equation

$$i\hbar \frac{d|\Psi\rangle}{dt} = H_{\text{eff}}|\Psi\rangle, \tag{14}$$

where $|\Psi\rangle = \alpha|g\rangle + \sum_{i=1}^{N} \beta_i|i\rangle$ and the effective Hamiltonian is

$$H_{\text{eff}} = \frac{\hbar\Omega_0}{2} \sum_i \left(e^{-i\mathbf{k}_0 \cdot \mathbf{r}_i} S_-^i + e^{i\mathbf{k}_0 \cdot \mathbf{r}_i} S_+^i\right) - \hbar\Delta_0 \sum_i S_+^i S_-^i - \frac{\hbar\Gamma}{2} \sum_j V_{ij} S_+^i S_-^j, \tag{15}$$

where

$$V_{ij} = (1 - \delta_{ij}) \frac{\cos(k_0|\mathbf{r}_i - \mathbf{r}_j|)}{k_0|\mathbf{r}_i - \mathbf{r}_j|} + i\frac{\sin(k_0|\mathbf{r}_i - \mathbf{r}_j|)}{k_0|\mathbf{r}_i - \mathbf{r}_j|}. \tag{16}$$

Assuming that at low saturation the system is weakly excited, so that $\alpha \approx 1$, the projection of Eq. (14) over the excited states $|i\rangle$ leads to Eq. (13). Is has been shown that this equation describes also the temporal evolution of N harmonic oscillators driven by the scalar electric field radiation E_0, as predicted by classical linear optics [9, 28]. It is important to notice that, even if the collective atomic state $|\Psi\rangle$ is entangled, the knowledge of only the probability amplitudes β_i obtained from the linear equations (13) is not by itself sufficient to detect entanglement, due to its classical nature. Conversely, entanglement could be observable in the solution of the master equation, even restricted to a single-excitation, since it contains correlations between atoms, and in particular between the ground state and the excited states.

Finally, we notice that the exact master equation (2) can be written in terms of the effective Hamiltonian (15), using Eqs. (14), (15) and $\rho = |\Psi\rangle\langle\Psi|$, as

$$\frac{d\rho}{dt} = \frac{1}{i\hbar} \left(H_{\text{eff}}\rho - \rho H_{\text{eff}}^\dagger\right) + \sum_i \sum_j \gamma_{ij} S_-^j \rho S_+^i. \tag{17}$$

The last term in Eq. (17) describes the refilling of the ground state due to spontaneous decay of the excited states, and is necessary to preserve the density operator trace equal to unity.

2.5 Timed Dicke state

Let us show how the steady state Eq. (6) provides an approximated solution of the single-excitation master equation. First, we observe that the external field couples the ground state $|G\rangle$ to the timed Dicke state $|TD\rangle$ defined in Eq. (5). The matrix elements involving the TD state are

$$\rho_{TD,G} = \langle TD|\rho|G\rangle = \frac{1}{\sqrt{N}}\sum_j e^{-i\mathbf{k}_0\cdot\mathbf{r}_j}\rho_{j,G}, \tag{18}$$

$$\rho_{TD,TD} = \langle TD|\rho|TD\rangle = \frac{1}{N}\sum_j\sum_m e^{-i\mathbf{k}_0\cdot(\mathbf{r}_j-\mathbf{r}_m)}\rho_{j,m}. \tag{19}$$

Their temporal evolutions are obtained from Eqs. (7)–(9) as

$$\frac{d\rho_{G,G}}{dt} = -i\frac{\sqrt{N}\Omega_0}{2}\left(\rho_{TD,G}-\rho_{G,TD}\right) + \sum_k\sum_l \gamma_{kl}\rho_{l,k}, \tag{20}$$

$$\frac{d\rho_{TD,G}}{dt} = \left(i\Delta_0 - \frac{\Gamma}{2}\right)\rho_{TD,G} - i\frac{\sqrt{N}\Omega_0}{2}\left(\rho_{G,G}-\rho_{TD,TD}\right)$$
$$-\frac{1}{\sqrt{N}}\sum_i e^{-i\mathbf{k}_0\cdot\mathbf{r}_i}\sum_{k\neq i}\left(\frac{\gamma_{ik}}{2}+i\Delta_{ik}\right)\rho_{k,G}, \tag{21}$$

$$\frac{d\rho_{TD,TD}}{dt} = -i\frac{\sqrt{N}\Omega_0}{2}\left(\rho_{G,TD}-\rho_{TD,G}\right)$$
$$+\frac{i}{N}\sum_i\sum_j e^{-i\mathbf{k}_0\cdot(\mathbf{r}_i-\mathbf{r}_j)}\left(\sum_{k\neq i}\Delta_{kj}\rho_{i,k}-\sum_{k\neq i}\Delta_{ik}\rho_{k,j}\right)$$
$$-\frac{1}{2N}\sum_i\sum_j\sum_k e^{-i\mathbf{k}_0\cdot(\mathbf{r}_i-\mathbf{r}_j)}\left(\gamma_{ik}\rho_{k,j}+\gamma_{kj}\rho_{i,k}\right). \tag{22}$$

These equations show explicitly the coupling induced by the laser between $|G\rangle$ and $|TD\rangle$. However, the dipole-dipole interactions and the cooperative decay favor the coupling also to all the other "subradiant" states $|s\rangle$, with $s = 1,\ldots,N-1$, completing the single-excitation Hilbert subspace. We make the assumption that all the matrix elements among these states $|s\rangle$ can be neglected, supposing that their occupation probability is small compared to the timed Dicke state. In practice, we assume

$$\rho_{i,G} = \langle i|TD\rangle\langle TD|\rho|G\rangle + \sum_s\langle i|s\rangle\langle s|\rho|G\rangle \approx \frac{1}{\sqrt{N}}e^{i\mathbf{k}_0\cdot\mathbf{r}_i}\rho_{TD,G}, \tag{23}$$

and

$$\rho_{i,j} = \langle i|TD\rangle\langle TD|\rho|TD\rangle\langle TD|j\rangle + \cdots \approx \frac{1}{N}e^{i\mathbf{k}_0\cdot(\mathbf{r}_i-\mathbf{r}_j)}\rho_{TD,TD}. \tag{24}$$

By substituting these expressions in Eq. (20)–(22) we obtain

$$\frac{d\rho_{G,G}}{dt} = -i\frac{\sqrt{N}\Omega_0}{2}\left(\rho_{TD,G}-\rho_{G,TD}\right)+\Gamma_N\rho_{TD,TD}, \tag{25}$$

$$\frac{d\rho_{TD,G}}{dt} = \left[i\Delta_N - \frac{\Gamma_N}{2}\right]\rho_{TD,G} - i\frac{\sqrt{N}\Omega_0}{2}\left(\rho_{G,G}-\rho_{TD,TD}\right), \tag{26}$$

$$\frac{d\rho_{TD,TD}}{dt} = -i\frac{\sqrt{N}\Omega_0}{2}\left(\rho_{G,TD}-\rho_{TD,G}\right)-\Gamma_N\rho_{TD,TD}, \tag{27}$$

where $\Delta_N = \Delta_0 - L_N$ and [13]

$$\Gamma_N = \frac{1}{N}\sum_i\sum_j \gamma_{ij} e^{-i\mathbf{k}_0\cdot(\mathbf{r}_i-\mathbf{r}_j)} = N\Gamma\langle|S_N(k_0,\theta,\phi)|^2\rangle_{\theta,\phi}, \tag{28}$$

$$L_N = -\frac{1}{N}\sum_i\sum_{j\neq i} \Delta_{ij} e^{-i\mathbf{k}_0\cdot(\mathbf{r}_i-\mathbf{r}_j)} = \frac{N\Gamma}{2\pi}\mathrm{P}\int_0^\infty d\kappa\frac{\kappa^3}{\kappa-1}\langle|S_N(k_0\kappa,\theta,\phi)|^2\rangle_{\theta,\phi}, \tag{29}$$

are the cooperative decay rate and the collective Lamb shift, respectively. In Eqs. (28) and (29) we introduced the structure function

$$S_N(\mathbf{k}) = \frac{1}{N}\sum_{j=1}^N e^{i(\mathbf{k}-\mathbf{k}_0)\cdot\mathbf{r}_j}, \tag{30}$$

and the average is taken over the total solid angle of emission of a photon with wave vector $\mathbf{k}$ at an angle θ with $\mathbf{k}_0$, where $|\mathbf{k}| = k_0$. Finally, the integral over κ in Eq. (29) is evaluated as a principal part.

Equations (25)–(27) have the form of optical Bloch equations for a two-level system with collective states $|G\rangle$ and $|TD\rangle$, interacting with a collective Rabi frequency $\sqrt{N}\Omega_0$, detuning Δ_N and linewidth Γ_N. The steady-state solution is given by,

$$\rho^s_{TD,G} = \frac{1}{1+s_c}\left(\frac{\sqrt{N}\Omega_0}{2\Delta_N+i\Gamma_N}\right), \tag{31}$$

$$\rho^s_{TD,TD} = \frac{1}{2}\left(\frac{s_c}{1+s_c}\right), \tag{32}$$

where

$$s_c = \frac{2N\Omega_0^2}{4\Delta_N^2+\Gamma_N^2} \tag{33}$$

is the collective saturation parameter. We recover the previous linear result of [10] in the limit $s_c \ll 1$, with a steady-state amplitude of the excited state

$$\beta_i \approx \left(\frac{\Omega_0}{2\Delta_N+i\Gamma_N}\right)e^{i\mathbf{k}_0\cdot\mathbf{r}_i} = \frac{\beta_{TD}}{\sqrt{N}}e^{i\mathbf{k}_0\cdot\mathbf{r}_i}. \tag{34}$$

We have numerically verified that the timed Dicke ansatz of Eqs. (23) and (24), or equivalently Eq. (34) in the linear regime, is a good approximation of the system when $b(\Delta_0) < 1$, where $b(\Delta_0) = b_0/[1 + (2\Delta_0/\Gamma)^2]$ is the optical thickness. Figure 2 shows a contour plot of the ratio P/P_{TD} ($P = \sum_j|\beta_j|^2$ and $P_{TD} = |\beta_{TD}|^2$, where β_j and β_{TD} have been obtained from the numerical solution of Eqs. (13) and from (34) respectively) as a function of N and Δ_0/Γ, for a Gaussian spherical distribution with parameter $k_0\sigma_R = 15$. For all values of $b(\Delta_0) < 1$, the excited state population is well described by the timed Dicke ansatz and yields a ratio $P/P_{TD} \sim 1$. This result is confirmed by the analysis of the standard deviation $\sigma_\beta = \sqrt{\langle|\tilde{\beta}|^2\rangle - |\langle\tilde{\beta}\rangle|^2}/|\langle\tilde{\beta}\rangle|$ of $\tilde{\beta} = \beta e^{-i\mathbf{k}_0\cdot\mathbf{r}}$ (see right Fig. 2 where the contour plot of σ_β is also showed). σ_β quantifies the deviation of the excitation field from the 'mean-field' timed-Dicke state: this deviation becomes significant when $b(\Delta_0)$ is larger than unity. Figure 2 (right) suggests that for large optical thickness the homogeneous approximation assumed in the timed Dicke ansatz (see Eq. (34)) is no more valid and a better description is demanded.
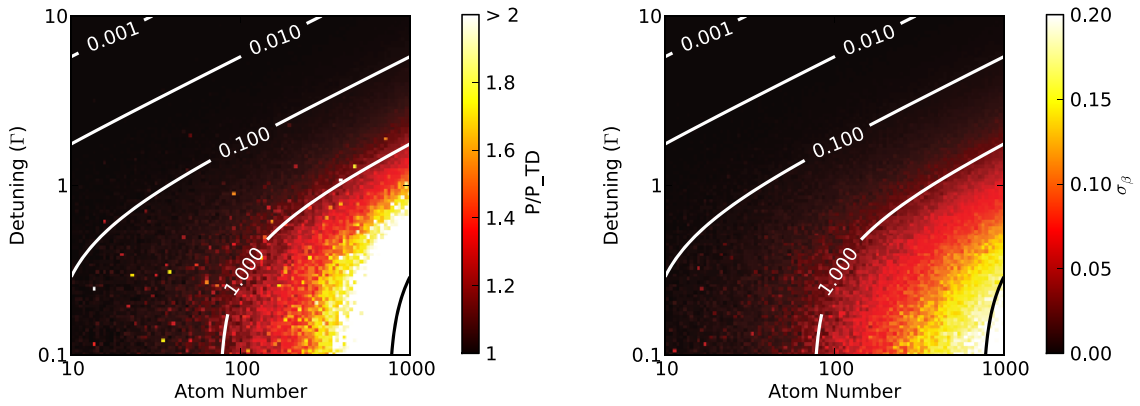
Fig. 2 (online colour at: www.fp-journal.org) Left: Ratio of the excited state population computed numerically and in the timed Dicke approximation P/P_{TD}. Right: Standard deviation σ_β. The cloud is Gaussian with $k_0\sigma_R = 15$. The contour plots show the iso-optical thickness lines $b(\Delta_0) = b_0/(1 + 4\Delta_0^2/\Gamma^2)$ where $b_0 = 3N/(k_0\sigma_R)^2$. This color-coded plot helps visualize the timed Dicke approximation validity region: $b(\Delta_0) < 1$.

2.6   Beyond the timed Dicke state approximation

To account for the non-uniformity of the excitation within the cloud, the field β can be decomposed as a sum of waves that describe its spatial fluctuations. This approach has been considered in [29], where Eq. (13) has been solved analytically for a continuous distribution with a Gaussian spherical profile, neglecting the cosine part of the exponential kernel and so the associated collective Lamb shift Δ_{ij}. Although the use of a such truncated kernel is not allowed when the decay of the excitation is observed [30], it may still provide a reasonable approximation for small density and low optical thickness $b(\Delta_0)$. The stationary excitation amplitude obtained in [29] using a partial wave expansion is

$$\beta(\mathbf{r}) = \Omega_0 \sum_{n=0}^{\infty} \frac{i^n(2n+1)}{2\Delta_0 + i\Gamma(1+\lambda_n)} j_n(k_0 r) P_n(\cos\theta), \tag{35}$$

where j_n are the spherical Bessel functions, P_n the Legendre polynomials, θ the angle with respect to the laser wave vector $\mathbf{k}_0$ and $\lambda_n = N(\pi/2\sigma^2)^{1/2}I_{n+1/2}(\sigma^2)\exp(-\sigma^2/2)$, where $\sigma = k_0\sigma_R$ and σ_R is the rms width of the Gaussian distribution. Equation (35) accounts for non-homogeneity of the excitation probability density $|\beta(\mathbf{r})|^2$. In this context, neglecting L_N, the timed Dicke expression (34) appears as a 'mean-field' approximation, which can be recovered assuming $\Gamma(1+\lambda_n) \sim \Gamma_N$ in Eq. (35). Going further beyond, an exact solution for the continuous-density limit of Eq. (13) with the exponential kernel has been derived using the Mie theory, although more mathematically demanding [31]. In that case, the excitation of an atom was calculated properly including both the incident and the phase-shifted radiation field from the other atoms.

3   Observables

3.1   Force on center of mass

Cooperative effects can be investigated by a direct detection of the scattered photons. However, this measurement can be in general difficult, since for an extended atomic system the emission is strongly forward directed and the detector can be saturated by the incident laser. The scattered radiation field detected at

distance $\mathbf{r}$ and time t is the sum of the single fields scattered by the N atoms of position $\mathbf{r}_j$,

$$E(\mathbf{r}, t) = \frac{dk_0^2}{2i\epsilon_0} \sum_{j=1}^{N} \frac{e^{-i\omega_0(t-|\mathbf{r}-\mathbf{r}_j|/c)}}{|\mathbf{r} - \mathbf{r}_j|} S_-^j(t). \tag{36}$$

In the far field limit, $|\mathbf{r} - \mathbf{r}_j| \approx r - (\mathbf{r} \cdot \mathbf{r}_j)/r$ and

$$E(\mathbf{r}, t) \approx \frac{dk_0^2}{2i\epsilon_0 r} e^{-i\omega_0(t-r/c)} \sum_{j=1}^{N} e^{-i\mathbf{k}\cdot\mathbf{r}_j} S_-^j(t), \tag{37}$$

where $\mathbf{k} = k_0(\mathbf{r}/r)$ and $\omega_0 = ck_0$, so that the average intensity is

$$I(\mathbf{r}, t) = \epsilon_0 c \langle E^\dagger(\mathbf{r}, t) E(\mathbf{r}, t) \rangle = \left(\frac{d^2\omega_0^4}{16\pi^2\epsilon_0 c^3 r^2} \right) \sum_j \sum_m e^{-i\mathbf{k}\cdot(\mathbf{r}_j - \mathbf{r}_m)} \rho_{j,m}(t). \tag{38}$$

Alternatively, it is relatively easier to detect the cooperative effects by considering the radiation pressure force exerted on the atoms. If the atoms are sufficiently cold, it is experimentally possible to measure the atomic motion after their exposition to the incident laser beam. The radiation pressure force acting on the jth-atom is $\hat{\mathbf{F}}_j = -\nabla_{\mathbf{r}_j} H = \hat{\mathbf{F}}_{aj} + \hat{\mathbf{F}}_{ej}$ where [10, 13]

$$\mathbf{F}_{aj} = i\hbar\mathbf{k}_0 \frac{\Omega_0}{2} \left\{ e^{i\Delta_0 t - i\mathbf{k}_0\cdot\mathbf{r}_j} S_-^j - e^{-i\Delta_0 t + i\mathbf{k}_0\cdot\mathbf{r}_j} S_+^j \right\}, \tag{39}$$

$$\mathbf{F}_{ej} = \mathbf{F}_{ej}^{(\text{self})} - \frac{\hbar k_0 \Gamma}{2} \sum_{m=1}^{N} \frac{\hat{\mathbf{r}}_{jm}}{(k_0 r_{jm})^2} \left\{ S_+^j S_-^m (1 - ik_0 r_{jm}) e^{ik_0 r_{jm}} + h.c. \right\}, \tag{40}$$

where $r_{jm} = |\mathbf{r}_j - \mathbf{r}_m| = |\mathbf{r}_{jm}|$ and $\hat{\mathbf{r}}_{jm} = \mathbf{r}_{jm}/r_{jm}$. $\mathbf{F}_{aj}$ and $\mathbf{F}_{ej}$ result from the recoil received upon absorption of a photon from the pump and from the emission of a photon into a direction $\mathbf{k}$, respectively. The emission force $\mathbf{F}_{ej}$ acting on the jth-atom has two contributions: a self-force $\mathbf{F}_{ej}^{(\text{self})} = -\hbar\Gamma \sum_{|\mathbf{k}|=k_0} \mathbf{k} S_+^j S_-^j$ due to its own photon emission, and a contribution accounting for the coupling between the jth-atom and all the other atoms. Note that the dipole-dipole interactions can occur via a coupling to common vacuum modes of radiation. The interference terms in the total scattered field can leave a fingerprint on the forces acting on the atoms inside the cloud. This force has a term decreasing as $1/r_{jm}$ and one decreasing as $1/r_{jm}^2$. Their average values on the single-excitation atomic states are

$$\langle \mathbf{F}_a^j \rangle = i\hbar\mathbf{k}_0 \frac{\Omega_0}{2} \left\{ e^{-i\mathbf{k}_0\cdot\mathbf{r}_j} \rho_{j,G} - c.c. \right\}, \tag{41}$$

$$\langle \mathbf{F}_e^j \rangle = -\frac{\hbar k_0 \Gamma}{2} \sum_{m=1}^{N} \frac{\hat{\mathbf{r}}_{jm}}{(k_0 r_{jm})^2} \left\{ \rho_{j,m}(1 - ik_0 r_{jm}) e^{ik_0 r_{jm}} + h.c. \right\}. \tag{42}$$

Notice that the self-force average to zero since the emission is isotropic. The force on the center-of mass of the atomic cloud, $\langle \mathbf{F} \rangle = (1/N) \sum_j \langle \mathbf{F}_j \rangle$ is of particular interest. From Eq. (41) and (42), its component along the z axis of incidence of the laser is

$$\langle \mathbf{F}_z \rangle = \frac{\hbar k_0}{N} \left\{ \Omega_0 \sum_j \text{Im}[\exp(i\mathbf{k}_0 \cdot \mathbf{r}_j)) \rho_{j,G}^*] - \Gamma \sum_{j,m} \hat{z}_{jm} j_1(k_0 r_{jm}) \text{Im}(\rho_{jm}) \right\}, \tag{43}$$

where $j_1(z) = \sin(z)/z^2 - \cos(z)/z$ is the first order spherical Bessel function and $\hat{z}_{jm} = (z_j - z_m)/r_{jm}$. In the timed-Dicke limit, using the approximations (23), (24) and neglecting saturation, Eq. (43) becomes [13]

$$\langle \mathbf{F}_z \rangle = \hbar k_0 \Gamma \frac{\Omega_0^2}{4\Delta_N^2 + \Gamma_N^2} N \left\langle (1 - \cos\theta)|S_N(\mathbf{k})|^2 \right\rangle_{\theta,\phi}. \tag{44}$$

The radiation pressure force can be influenced by different effects. On one side, the finite extent of the atomic cloud can produce strong forward oriented scattering. The balance between the momentum of the incident and scattered photons and the atoms indicate that for forward emission, the net recoil imprinted onto the atoms is vanishing, resulting in a reduction of the radiation force. A different contribution to the reduction of the radiation force can be seen in the prefactor of Eq. (44), which would appear even in the case of isotropic scattering (i.e. when $\langle \mathbf{F}_e \rangle = 0$). The importance of this prefactor can be understood from the cooperative coupling of several atoms into the same vacuum mode. The number of available modes for large spherical clouds can be estimated by $N_m \sim (k_0 R)^2$ (where R is the cloud's size), resulting in a number of atoms per mode scaling as $N/N_m \sim N/(k_0 R)^2$. This scaling is conveniently related to the on-resonant optical thickness of the atomic cloud b_0. For a Gaussian density distribution with root mean square size σ_R, $b_0 = 3N/(k_0\sigma_R)^2$, $N\langle|S_N|^2\rangle_{\theta,\phi} = 1 + b_0/12$ and $N\langle(1-\cos\theta)|S_N|^2\rangle_{\theta,\phi} = b_0/24(k_0\sigma_R)^2$ [10].

It is convenient to compare the cooperative radiation pressure force to the force acting on a single independent atom $F_{\text{ind}} = \hbar k_0 \Gamma \Omega_0^2 / (\Gamma^2 + \Delta_0^2)$. The ratio of the cooperative radiation pressure force for a Gaussian cloud to the single-atom force in the timed Dicke limit can be written as (neglecting the collective Lamb shift)

$$\frac{F_z}{F_{\text{ind}}} = \frac{4\Delta_0^2 + \Gamma^2}{4\Delta_0^2 + \left(1 + \frac{b_0}{12}\right)^2 \Gamma^2} \left[1 + \frac{b_0}{24(k_0\sigma_R)^2}\right]. \tag{45}$$

One can also use the partial wave expansion to account for the inhomogeneity of the field β, in which case the force ratio reads [29]:

$$\frac{F_z}{F_{\text{ind}}} = \frac{\Gamma^2 + \Delta_0^2}{N} \tag{46}$$

$$\times \sum_{n=0}^{\infty} \left(\frac{(2n+1)\lambda_n(1+\lambda_n)}{4\Delta_0^2 + \Gamma^2(1+\lambda_n)^2} - \frac{(2n+2)\lambda_n\lambda_{n+1}[4\Delta_0^2 + \Gamma^2(1+\lambda_n)(1+\lambda_{n+1})]}{[4\Delta_0^2 + \Gamma^2(1+\lambda_n)^2][4\Delta_0^2 + \Gamma^2(1+\lambda_{n+1})^2]} \right).$$

Figure 3 shows the ratio of the cooperative to independent radiation pressure force as a function of the atom number N and detuning Δ_0 for a Gaussian cloud with root mean square size $k_0\sigma_R = 10$. The left figure shows the numerical results computed from the effective Hamiltonian equation (15) and Eq. (43), the central one describes the timed-Dicke formula Eq. (45) and the right picture stands for the partial wave equation (**??**). While all methods predict a significant reduction of the force ratio for small detuning and large atom number, the partial wave approach yields better agreement with the numerical approach for $\Delta_0 < \Gamma$ and $N > 1000$, despite the fact that the present partial wave approach has been limited to a sine kernel, not fully accounting for virtual-transition induced phase shifts [30].
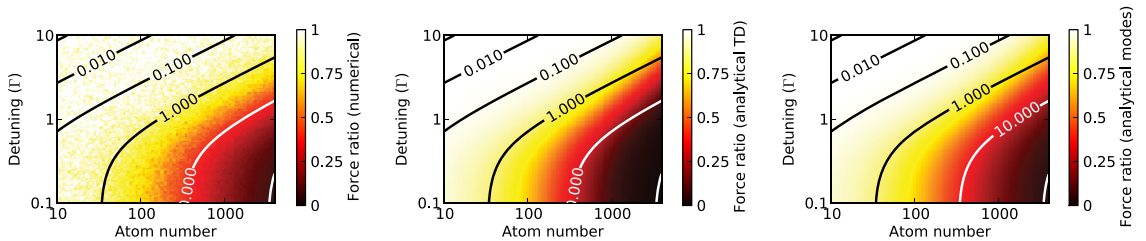

Fig. 3 (online colour at: www.fp-journal.org) Ratio of the cooperative to independent radiation pressure force as a function of the atom number N and detuning Δ_0. The cloud is Gaussian with $k_0\sigma_R = 10$. The contour plots show the iso-optical thickness lines $b(\Delta_0) = b_0/(1 + 4\Delta_0^2/\Gamma^2)$ where $b_0 = 3N/(k_0\sigma_R)^2$. The left figure shows the numerical results computed from the effective Hamiltonian equation (15) and Eq. (43), the central figure stands for the analytical formula Eq. (45) and the right figure correspond to the modal expansion (**??**).

3.2   Dicke subradiance

Dicke subradiance is the counterpart of superradiant emission and corresponds to the partial trapping of light due to destructive interferences. In a subradiant state, the atomic dipoles are arranged such that the macroscopic polarization of the cloud is small reducing the emission rate of the system. Subradiant emission has been previously observed for two ions [32] and also for the emission of a cloud of N atoms in a free space into a single radiation mode [33]. In a recent paper [26], we showed that the system presented above is ideal to observe for the first time long photon storage into metastable subradiant states for N atoms in free space.

In Sect. 2.5, we saw that the laser pumps the system from the ground state $|G\rangle$ into the timed Dicke state $|TD\rangle$. Then the dipole-dipole interaction terms couple the timed Dicke state to the different other states of the system. Some of these states $|\psi_{\text{super}}\rangle$ have short lifetimes $\Gamma_{\text{super}} > \Gamma$ and are thus called *superradiant*.
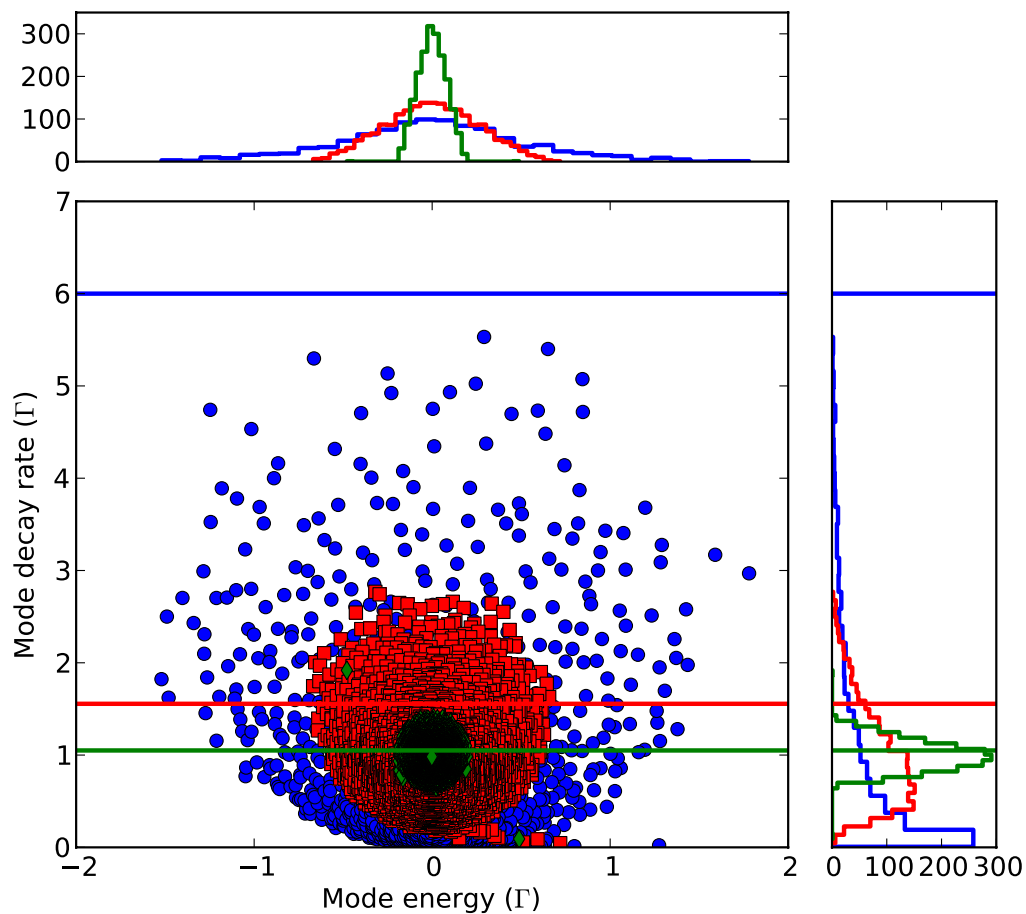

Fig. 4   (online colour at: www.fp-journal.org) Energies and decay rates of the modes of the system obtained by computing the eigenvalues of the effective Hamiltonian H_{eff} for Gaussian clouds with $N = 2000$ atoms and $k_0 \sigma_R = 10, 30, 100$ ($b_0 = 60, 6.7, 0.6$) given respectively by the blue, red and green curves. The denser the system is, the wider the energy and decay rate distributions are. The continuous straight lines show the timed Dicke state decay rates Γ_N for the three different system sizes. For dilute clouds (green line), the timed Dicke emission rate Γ_N is centered on the distribution $P(\Gamma)$ and $\Gamma_N \simeq \Gamma$. When the cloud optical density increases (blue line), the timed Dicke decay rate tends to the tail of the distribution and $\Gamma_N \simeq \Gamma_{\text{max}}$.

Some other states $|\psi_{\text{sub}}\rangle$ have long lifetimes $\Gamma_{\text{sub}} < \Gamma$ and are called *subradiant*. As the effective Hamiltonian is non-Hermitian, its eigenstates are not orthogonal and have common features with autoionizing states or Fano resonances [23]. Figure 4 shows the mode energies and decay rates for three different system sizes. It shows that the denser the system is, the wider the energy and decay rate distributions are. Figure 4 also shows the timed Dicke decay rate Γ_N to compare it to the decay rate distribution of the system modes $P(\Gamma)$. For dilute clouds, the timed Dicke emission rate Γ_N is centered on the distribution $P(\Gamma)$ and $\Gamma_N \simeq \Gamma$ and when the cloud optical density increases, the timed Dicke decay rate tends to the tail of the distribution and $\Gamma_N \simeq \Gamma_{\text{max}}$.
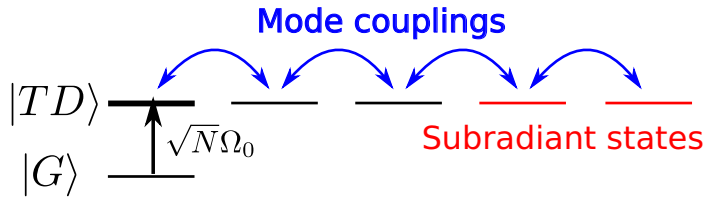

Fig. 5   (online colour at: www.fp-journal.org) Sketch of the subradiant emission couplings.

After driving the system with the laser for a long time, which allows populating subradiant states using the scheme sketched in Fig. 5, we monitor the decay of the system by looking at the excited state population $P(t)$ after switching off the laser. A typical decay curve of the excited state population computed from the numerical solution of the effective Hamiltonian approach is shown on Fig. 6. This figure shows the excitation probability $P(t) = \sum_j |\beta_j|^2$ as a function of time (black solid line), obtained by integrating Eq. (13) for $N = 2000$ atoms distributed by a Gaussian distribution with $k_0\sigma_R = 10$. The other parameters are $\Omega_0 = 0.01\Gamma$ and $\Delta_0 = 10\Gamma$ and the laser is switched off after $t = 50\Gamma^{-1}$. The origin of time is set such that it corresponds to the time when the laser is switched off. Under the action of the continuous laser excitation, the atoms reach a quasi-stationary state close to the timed Dicke state. The small subradiant
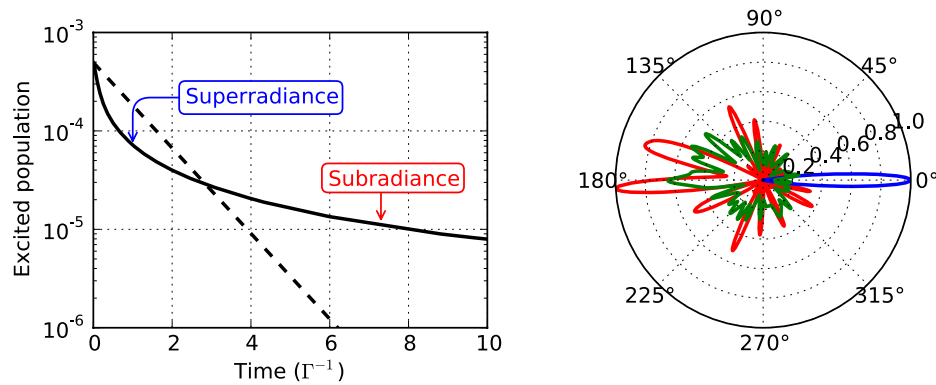

Fig. 6   (online colour at: www.fp-journal.org) Excited state population $P = \sum_j |\beta_j|^2$ decay after switching off the laser (the initial state corresponds to the steady state. The black dashed curve shows the single atom decay (without cooperative effects). At first, the fast decay corresponds to superradiance with a rate $\Gamma_N = (1 + b_0/12)\Gamma$. After some time, part of the light remains trapped in the cloud which corresponds to subradiant emission. Parameters for the simulation: $N = 2000$, $k_0\sigma_R = 10$, $\Omega_0 = 0.01\Gamma$, $\Delta_0 = 10\Gamma$ (the laser was on before during $50\Gamma^{-1}$ to let the system reach the steady state). The superradiant emission diagram (blue curve) is strongly forward directed. The emission diagram of the subradiant states (red curve) is isotropic. The green curve shows the subradiant emission diagram averaged over eight realizations of disorder.

fraction present in the atomic state after the exposition to the laser can be detected observing the excitation decay after the laser has been switched off. The fast initial decay rate of the superradiant state is $\Gamma_N = (1 + b_0/12)\Gamma$ as expected since the steady state corresponds approximately to the timed Dicke state. After some time, the emission rate becomes much below the single atom emission rate (black dotted line in Fig. 6). It corresponds to the subradiant emission region. At first, the subradiant decay is not exponential since several modes decay simultaneously. For longer times, it then ends up with a pure exponential decay, referred as the subradiant decay rate, when only one long-lived mode dominates [26, 28], as shown in the red part of the decay curve of Fig. 7. We have checked numerically the very intuitive result that the subradiant decay rate measured on the relaxation curves $P(t)$ corresponds to the longest lifetime of the effective Hamiltonian modes [28]. This confirms the role of cooperativity in long lived excitations in the cloud as investigated in [34].
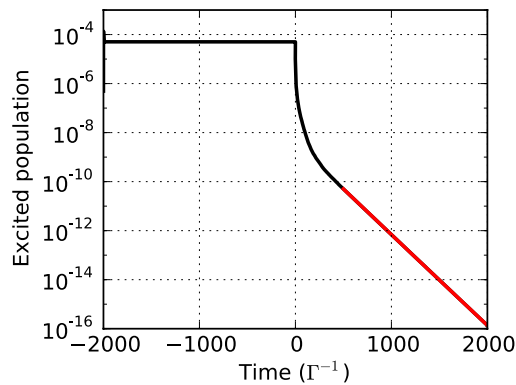

Fig. 7 (online colour at: www.fp-journal.org) Excited state population as a function of time for the same parameters as Fig. 6 ($N = 2000$, $k_0\sigma_R = 10$, $\Omega_0 = 0.01\,\Gamma$, $\Delta_0 = 10\,\Gamma$). The laser is switched off at $t = 0$. The curve together with Fig. 6 show that the subradiant decay is purely exponential only after a certain amount of time (red part of the curve), when the mode with the longest lifetime dominates. We call this final decay rate the subradiant decay rate. In this example, $\Gamma_{\text{sub}} = 8.5\,10^{-3}\,\Gamma$.

Using Eq. (38) from the previous section, we can study the emission diagram of the system. Fig. 6 shows the emission diagram as a function of time during the decay of the cloud. At first, the emission diagram of the timed Dicke state is clearly forward directed, a phenomenon reminiscent of Mie scattering. At longer times, subradiant modes show isotropic emission diagrams: they do not possess the symmetry of the laser excitation since they are not directly coupled to it. This property can be exploited in the experimental detection of subradiance.

In [26], we proposed to use inhomogeneous broadening schemes such as the cloud optical thickness, the cloud temperature, or the driving laser intensity as possible control parameters for subradiance. However, other parameters such as a far detuned speckle field, magnetic fields, or near field couplings can also be used. By control of subradiance, we mean two different things: controlling the population of the subradiant states as well as their decay rates. Exploiting these inhomogeneous broadening schemes allow to control and tune the dipole-dipole couplings, which is the genuine interaction leading to cooperative effects (superradiance, subradiance, cooperative Lamb shift). This would allow for the first observation of subradiant emission from a cloud of atoms in free space.

3.3 Dipole-dipole induced suppression of excitation

In the perturbative limit, where each dipole is driven by the external field, plus a small perturbation by the field scattered by all other dipoles, we can obtain an analytical solution of the excitation state population and the angle-resolved scattered field.

From Eq. (38) we obtain the steady-state scattered intensity in the direction (θ, ϕ) for the timed Dicke state, still neglecting saturation:

$$I(r, \theta, \phi) = \left(\frac{I_0}{16\pi^2 k_0^2 r^2} \right) \frac{\Gamma^2 N^2 |S_N(\theta, \phi)|^2}{4\Delta_N^2 + \Gamma_N^2}. \tag{47}$$

and the total scattered intensity

$$P_s = r^2 \int_0^{2\pi} d\phi \int_0^{\pi} d\theta \sin\theta \, I(r,\theta,\phi) = P_0 \frac{N\Gamma\Gamma_N}{4\Delta_N^2 + \Gamma_N^2}, \tag{48}$$

where I_0 is the incident intensity and $P_0 = I_0/(4\pi k_0^2)$. In Fig. 8, we plot the normalized excited state population (blue solid line on the left figure) as a function of b_0 and for $\Delta_0 = 100\Gamma$,

$$\frac{P}{NP^{(1)}} = \frac{4\Delta_0^2 + \Gamma^2}{4\Delta_N^2 + \Gamma_N^2} \approx \frac{4\Delta_0^2 + \Gamma^2}{4\Delta_0^2 + \Gamma^2(1 + b_0/12)^2}, \tag{49}$$

and the normalized total scattered power (blue solid line on the left figure)

$$\frac{P_s}{NP_0} \approx \frac{\Gamma^2}{4\Delta_0^2 + \Gamma^2(1 + b_0/12)^2}(1 + b_0/12), \tag{50}$$

where $P^{(1)} = \Omega_0^2/(4\Delta_0^2 + \Gamma^2)$ is the single-atom excitation probability and we have neglected the collective Lamb shift, $\Delta_N \approx \Delta_0$. We observe that increasing the optical thickness b_0 the excitation population decreases, whereas the total scattered power has a maximum around $b_0 \sim 24(\Delta_0/\Gamma)$. The normalized excited state population and total scattered power resulting from the partial wave solution (35) in the continuous-density approximation, obtained in [29] for large Gaussian clouds,

$$\frac{P}{NP^{(1)}} = \frac{4\Delta_0^2 + \Gamma^2}{\Delta_0\Gamma(b_0/3)} \arctan\left[\frac{\Delta_0\Gamma(b_0/3)}{4\Delta_0^2 + \Gamma^2(1 + b_0/6)}\right], \tag{51}$$

and

$$\frac{P_s}{NP_0} = \frac{3}{b_0} \ln\left[1 + \frac{\Gamma^2 b_0}{3} \frac{1 + b_0/12}{4\Delta_0^2 + \Gamma^2}\right], \tag{52}$$

are also plotted in Fig. 8 (red dashed lines): they show a deviation from the timed Dicke approximation for very large resonant optical thickness b_0.

From these curves we can see that even for dilute clouds of cold atoms, the long range coupling between the dipoles leads to a cooperative modification of the excitation of the atoms and its related total scattered power. Note that the total scattered power initially increases with increasing number of atoms, despite the
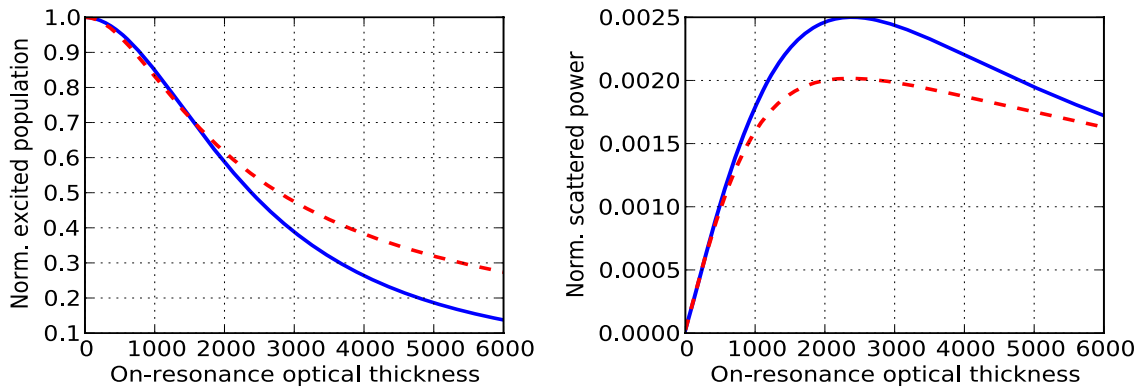

Fig. 8 (online colour at: www.fp-journal.org) Normalized excited state population (left) and normalized total scattered power (right) as a function of the optical thickness b_0 for $\Delta_0 = 100\,\Gamma$. The blue solid lines correspond to Eqs. (49), (50) and the red dashed lines to Eqs. (51), (52).

decrease in the normalized total population of the excited state. This can be understood by the fact that cooperativity leads to enhanced superradiant emission rates. For larger number of atoms, the suppression of the atomic excitation dominates the enhanced superradiant emission and the total scattering rate of the large cloud of atoms is reduced by the dipole-dipole couplings. We stress that even though the signature of such a suppression of fluorescence of the cloud of N atoms might bear a resemblance with a photon blockade regime [16–18], our model does not take into account optical nonlinearities required to describe such photon-photon coupling. A suppression of excitation can thus be obtained in the absence of nonlinear optical response. In contrast to dipole blockade effects in Rydberg states with near-field ($1/r^3$) or Van der Waals coupling ($1/r^6$), we are in the presence of long-range dipole-dipole couplings where all atoms participate in the suppression of the atomic excitation, and not only a small volume around an excited atom.

4 Conclusion

In this paper, we have presented a master equation and an effective Hamiltonian approach to describe cooperative effects in clouds of cold atoms. This master equation approach, even though still restricted to single excitation, allows to go beyond the effective Hamiltonian approach. In particular, we have highlighted the possibility of cooperative suppression of the atomic excitation, via the long range dipole-dipole couplings and in the absence of any non-linear photon blockade mechanism. Future work will include the possibility of experimental observation of Dicke subradiance, long range dipole-dipole blockade and cooperative effects beyond linear optics.

References

 [1] R. H. Dicke, Phys. Rev. **93**, 99 (1954).
 [2] J. Javanainen, Phys. Rev. Lett. **72**, 2375 (1994).
 [3] J. M. Raimond et al., Phys. Rev. Lett. **49**, 117 (1982).
 [4] J. P. Hannon and G. T. Trammell, Hyperfine Interactions **123/124**, 127 (1999).
 [5] R. Röhlsberger et al., Science **328**, 1248–1251 (2010).
 [6] M. O. Scully, E. S. Fry, C. H. R. Ooi, and K. Woďkiewicz, Phys. Rev. Lett. **96**, 010501 (2006).
 [7] J. H. Eberly, J. Phys. B, At. Mol. Opt. Phys. **39**, S599 (2006).
 [8] A. A. Svidzinsky, J.-T. Chang, and M. O. Scully, Phys. Rev. Lett. **100**, 160504 (2008).
 [9] A. A. Svidzinsky, J.-T. Chang, and M. O. Scully, Phys. Rev. A **81**, 053821 (2010).
[10] Ph. W. Courteille, Eur. Phys. J. D **58**, 69 (2010).
[11] T. Bienaimé et al., Phys. Rev. Lett. **104**, 183602 (2010).
[12] H. Bender et al., Phys. Rev. A **82**, 011404 (2010).
[13] T. Bienaimé et al., J. Mod. Opt. **58**, 1942 (2011).
[14] M. Tiersch, S. Popescu, and H. J. Briegel1, arXiv:1104.3883v.
[15] F. Bariani and T. A. B. Kennedy, Phys. Rev. A **85**, 033811 (2012).
[16] D. Tong et al., Phys. Rev. Lett. **93**, 063001 (2004).
[17] K. Singer et al., Phys. Rev. Lett. **93**, 163001 (2004).
[18] M. Saffman, T. G. Walker, and K. Molmer, Rev. Mod. Phys. **82**, 2313 (2010).
[19] G. S. Agarwal, Quantum Statistical Theories of Spontaneous Emission and their Relation to other Approaches, in: Springer Tract in Modern Physics, edited by G. Höhler (Springer-Verlag, Berlin, 1974).
[20] S. Das, G. S. Agarwal, and M. O. Scully, Phys. Rev. Lett. **101**, 153601 (2008).
[21] M. O. Scully, Phys. Rev. Lett. **102**, 143601 (2009).
[22] R. Friedberg, S. R. Hartman, and J. T. Manassah, Phys. Rep. **7**, 101 (1973).
[23] U. Fano, Phys. Rev. **124**, 1866 (1961).
[24] F. W. Cummings, Phys. Rev. A **33**, 1683 (1986).
[25] M. O. Scully and A. A. Svidzinsky, Phys. Rev. Lett. **373**, 1283 (2009).

[26] T. Bienaimé, N. Piovella, and R. Kaiser, Phys. Rev. Lett. **108**, 123602 (2012).

[27] A. Gaëtan et al., Nature (Phys. Sci.) **5**, 115 (2009).

[28] T. Bienaimé, Ph.D. thesis (Université de Nice Sophia Antipolis, Nice, 2011).

[29] R. Bachelard, N. Piovella, and Ph. W. Courteille, Phys. Rev. A **84**, 013821 (2011).

[30] J. T. Manassah, Phys. Rev. A **85**, 015801 (2012).

[31] R. Bachelard, Ph. W. Courteille, R. Kaiser, and N. Piovella, Eur. Phys. Lett. **97**, 14004 (2012).

[32] R. G. DeVoe and R. G. Brewer, Phys. Rev. Lett. **76**, 2049 (1996).

[33] D. Pavolini et al., Phys. Rev. Lett. **54**, 1917 (1985).

[34] E. Akkermanns, A. Gero, and R. Kaiser, Phys. Rev. Lett. **101**, 103602 (2008).